Document downloaded from:

http://hdl.handle.net/10251/61197

This paper must be cited as:

Sánchez Tovar, R.; Montañés Sanjuan, MT.; Garcia-Anton, J.; Abdellah; Guenbour, A. (2012). Influence of temperature and hydrodynamic conditions on the corrosion behavior of AISI 316L stainless steel in pure and polluted H3PO4: Application of the response surface methodology. Materials Chemistry and Physics. 133(1):289-298. doi:10.1016/j.matchemphys.2012.01.024.

The final publication is available at

http://dx.doi.org/10.1016/j.matchemphys.2012.01.024

Copyright Elsevier

Additional Information

*Manuscript
Click here to view linked References

Influence of temperature and hydrodynamic conditions on the corrosion behaviour of AISI 316L stainless steel in pure and polluted H_3PO_4. Application of the response surface methodology

[1]R. Sánchez-Tovar, [1]M.T. Montañés, [1]J. García-Antón, [2]A. Guenbour

[1]Ingeniería Electroquímica y Corrosión, Dep. Ingeniería Química y Nuclear, Universitat Politècnica de València, Camino de Vera s/n, 46022 Valencia, Spain; tel. +34963877632; fax: +34963877639; e-mail: jgarciaa@iqn.upv.es

[2]Laboratoire de Corrosion-Electrochimie, Faculté des Sciences, Université Mohammed V-Agdal, BP 1014 Rabat, Morocco.

Abstract

The cost associated with corrosion is an issue of major economic importance; controlling corrosion would promote the conservation of natural resources in relation to metals and save both energy and water. Phosphoric acid is mainly produced by the wet acid process, where corrosion problems could be intensified due to the presence of impurities in the phosphate rock. Operating temperatures and flowing conditions aggravate the aforementioned problems. This work studies the influence of temperature (25 to 60 ºC) and hydrodynamic conditions (Reynolds numbers from 1456 to 5066) on the corrosion of AISI 316L stainless steel in pure and polluted phosphoric acid solutions, by means of cyclic potentiodynamic polarization curves in a hydrodynamic circuit. The effect of temperature is the same as that caused by impurities; that is, higher corrosion rates and hindered passivation and repassivation resistance of the alloy. Statistical analysis by means of surface response methodology proved that the effect of temperature on the corrosion parameters of ASI 316L is more influential than the Reynolds number effect. The Reynolds number seems to have no significant

influence on the corrosion behaviour of stainless steel. Furthermore, the influence of temperature on the corrosion rate is much higher than on the rest of the corrosion parameters analysed, especially in polluted phosphoric acid solutions. AISI 316L stainless steel has a clear interest for the phosphoric acid industry as a component material of some equipment due to its good corrosion properties at the different temperatures and Reynolds numbers studied even in polluted media.

Keywords: A. alloys; C. corrosion test; C. electrochemical techniques; D. corrosion

1. Introduction

More than 95% of the world's phosphoric acid production is by the wet acid process. Wet phosphoric acid manufacturing appears to be relatively simple involving the reaction of phosphate rock with concentrated sulphuric acid yielding phosphoric acid (26 to 28% P_2O_5) and calcium sulphate slurry, followed by filtration of the acid slurry to remove particulate matter, and by concentration and purification of the phosphoric acid. Although the process is simple and straightforward, severe erosion/corrosion problems have been encountered. Corrosion problems occur due to impurities in the phosphate rock, such as chlorides (Cl^-) in presence of sulphuric acid (H_2SO_4) traces. In fact, sulphuric acid is the most common impurity in the wet acid process since this compound is necessary in a certain excess [1]. Chloride promotes pitting corrosion; moreover, the effects of chloride are intensified by the presence of sulphuric acid. The recent trend to increase the concentration of the final product involves using higher operating temperatures. This fact, along with the hydrodynamic operating conditions prevailing in these plants, increases the severity of the corrosive environments [2-5].

Corrosion can be defined as the destruction or deterioration of a metallic material by reaction with its environment. This process can affect the mechanical integrity of facilities and damage the quality of the end products by contamination with the resulting corrosion compounds. All these facts lead to substantial economic losses; hence, the importance of studying corrosion to reduce material losses in the industrial sector, as well as to promote the conservation of natural resources, particularly metals, but would finally result in save both energy and water. The estimated annual direct cost of corrosion in the U.S. is about 276 billion dollars, approximately 3.1% of the nation's Gross Domestic Product (GDP) [6]. Thus, the costs of metal and metal alloy corrosion amount to several percent of the GDP of an industrialized country are an issue of major economic importance [7].

Austenitic stainless steels (SS) are widely used in many industrial areas where high corrosion resistance is required [8-11], for instance in the phosphoric acid industry [12]. In particular, AISI 316L stainless steel is widely used due to its good mechanical properties and corrosion resistance [13].

Few works have addressed the influence of impurities on the corrosion behaviour of austenitic stainless steels in phosphoric acid solutions [14-16] and none of them has studied the hydrodynamic conditions, which are the real conditions for the productionof phosphoric acid. Some works have studied the effects of temperature on different materials in polluted phosphoric acid solutions under static conditions: graphite [2], stainless steels and graphite [17], austenitic stainless steels [18], mild steel [19] and Ti-Cu [20]. On the other hand, very few works have analysed the corrosion-erosion behaviour in polluted phosphoric acid media [4]. Therefore, the first aim of this work is the study of the influence of the operating conditions (temperature: 25, 40 and 60 ºC and Reynolds number: 1456, 3166 and 5066) on the

corrosion of AISI 316L SS tubes in pure and polluted (with impurities of H_2SO_4 and Cl^-) phosphoric acid solutions using a hydrodynamic circuit. Cyclic polarization curves were performed to study the corrosion behaviour of the alloy. Potentiodynamic procedures are widely used to determine the electrochemical corrosion behaviour of an active-passive material [21, 22].

Response surface methodology (RSM) is a powerful experimental design tool [23] and has been successfully employed for the statistical analysis of different systems, some of which related to the corrosion field; for example RSM was used to evaluate the conditions for the high-dose polyphosphate inhibition in reducing copper release [24]. The feasibility of using a higher dosage of polyphosphate was of interest because it could reduce copper release from corroded copper pipes within a short period by forming the protective film. Rajakumar [25] employed RSM to analyse the relationships between the friction stir welding input parameters (rotational speed, welding speed, axial force, shoulder diameter, pin diameter and tool hardness) and three output responses (tensile strength, hardness and corrosion rate). RSM was also used by Masmoudi [26] to determine the effects of the passivating solution concentration, temperature and period of treatment on the corrosion resistance of passivated commercially pure titanium and the Ti_6Al_4V alloy. Thus, the second aim of this study is the performance of a RSM-based statistical analysis in order to evaluate the combined effects of temperature and Reynolds number on the main corrosion parameters (corrosion potential, corrosion current density, passivation current density and breakdown potential), and to find out which of these operating conditions is more influential on the corrosion behaviour of AISI 316L stainless steel. The presence of impurities was also taken into consideration.

2. Materials and methods

2.1. Materials characterisation

The materials studied were tubes 14 mm and 16 mm in inner and external diameter, respectively, and 20 mm in length (an area of 8.8 cm^2 was exposed to the solution). They were made of AISI 316L SS (16.957 wt. % Cr, 10.171 wt. % Ni, 1.337 wt. % Mn, 2.298 wt. % Mo, 0.004 wt. % S, 0.368 wt. % Si, 0.030 wt. % P, 0.022 wt. % C, bal. wt. % Fe). For the characterisation of the AISI 316L stainless steel, microstructure and microhardness analyses were carried out.

To observe the microstructure of the alloy, the tubes were cut lengthwise and covered in cold mounting acrylic resin for the embedding of the specimens. Then, the samples were wet abraded from 220 silicon carbide (SiC) grit to 4000 SiC grit (in several steps; i.e. 220, 500, 1000, 2500 and 4000). Finally, the mounted samples were polished with 1 and 0.3 micron alumina and were rinsed with distilled water, followed by ethanol. Once the samples were polished, metallographic etching (Kiesel modified) was carried out according to ASM International [27]. The etchant composition consisted of 10 mL of nitric acid (65 wt. %), 10 mL of acetic acid (99-100 wt. %), 15 mL of hydrochloric acid (37-38 wt. %) and 5 mL of glycerine (100 wt. %). The samples were immersed in the etching solution during 90 seconds and then rinsed with distilled water, followed by ethanol. Subsequently the materials were examined by scanning electron microscopy (SEM) and light microscopy (LM) to reveal their microstructure.

Vickers microhardness measurements were carried out using a microhardness tester (Struers Duramin) with a diamond pyramid indenter at a load of 300 g for 15 s [28]. Hardness values were obtained as the mean of six readings.

2.2. Solution

The materials were tested in a 5.5 M H_3PO_4 solution (40 wt. % H_3PO_4) made with distilled water. This concentration is typical in the phosphoric acid industry [1]. In order to study the effect of impurities on the corrosion of AISI 316L stainless steel tubes, a polluted phosphoric acid solution was used. Table 1 shows the composition of the different phosphoric acid solutions employed in this work.

The experiments were conducted at Reynolds numbers of 1456, 3166 and 5066 at 25 ºC, 40 ºC and 60 ºC. Reynolds numbers were calculated as follows:

$$\mathrm{Re} = \frac{v \cdot d \cdot \rho}{\mu} \tag{1}$$

where v is the characteristic fluid velocity in $m \cdot s^{-1}$, d is the characteristic length of the system in m (the diameter of a pipe in the case of pipe flow), ρ is fluid density in $Kg \cdot m^{-3}$ and μ is the dynamic fluid viscosity in $Kg \cdot m^{-1} \cdot s^{-1}$.

The density values of the phosphoric acid solutions at the different temperatures studied are presented in Table 2 [29-31]. The density of the polluted phosphoric acid solutions was determined from the density values of the different compounds that form the polluted solution at the corresponding temperature (see Table 2) according to equation 2 [32]:

$$\rho_m = \frac{1}{\omega_{H_2O} \cdot \bar{v}_{H_2O} + \omega_i \cdot \bar{v}_i} \tag{2}$$

where ρ_m is the density of the mixture in $Kg \cdot m^{-3}$, ω_{H_2O} is the mass fraction of water, $\bar{v}_{H_2O}$ is the water specific volume in $m^3 \cdot Kg^{-1}$, ω_i is the mass fraction of component i and $\bar{v}_{H_2O}$ is the specific volume of component i in $m^3 \cdot Kg^{-1}$.

The viscosity values of the phosphoric acid solutions at the different temperatures were obtained experimentally with a Cannon-Fenske viscosimeter [33, 34] and a thermostat. As density and viscosity values change with temperature, the rates equivalent to the applied Reynolds numbers (1456, 3166 and 5066) are summarized in Table 3.

2.3. Hydrodynamic circuit

Figure 1 shows the hydrodynamic circuit used to study corrosion under flowing conditions. It consists of a centrifugal pump (piece J in Figure 1), a flow-meter (piece A in Figure 1), a thermostat to regulate the solution temperature (piece H in Figure 1), a test section (where the tube is assessed, piece B in Figure 1), a valve to drain the system (piece I in Figure 1) and several glass devices: for the reference electrode (Ag/AgCl, 3M KCl; piece C in Figure 1), for the auxiliary electrode (Pt; piece D in Figure 1), for the gas output (piece E in Figure 1), to introduce the solution into the flow circuit (piece F in Figure 1) and to bubble an inert gas (piece G of Figure 1). Medical grade silicone flexible tubes were used to assemble the different elements. Fully developed flow was assured using a 90-cm-long Teflon rigid tube of the same inner diameter as the test tube upstream of the test section.

Before each test the tubes were degreased with ethanol and dried with air at room temperature. Nitrogen (99.99 %) was bubbled into the solution for 60 minutes. The hydrodynamic circuit was purged with nitrogen using a glass adapter for 20 minutes. Then, the hydrodynamic circuit was tight closed to maintain these conditions. All the tests were

repeated at least three times for reproducibility. After the tests, the tubes were rinsed with ethanol and dried with air at room temperature. Then, the samples were cut lengthwise to observe the surface exposed to the acid solutions. To this end, a laser scanning confocal microscope (LSCM) Olympus LEXT OLS3100, which utilized LEXT OLS 6.0.3 software, was used. The LSCM uses a Laser Diode with a wavelength of 408 nm, an outstanding horizontal resolution of 0.22 μm, vertical resolution of 0.01 μm (z-axis), and a magnification range from 120x to 14400x.

2.4. Electrochemical tests

Cyclic polarization curves were used to study the hydrodynamic corrosion of AISI 316L SS in the different acid solutions. To perform the tests a potentiostat (Solartron 1285 provided with the Corrware software) was used. Before obtaining the cyclic potentiodynamic curves, the open circuit potential (OCP) was recorded for one hour. After the OCP test, the potential was reduced progressively to -400 $mV_{Ag/AgCl}$; then, the working electrode potential was scanned from -400 $mV_{Ag/AgCl}$ to the anodic direction until the current density reached 0.2 mA/cm^2, where the potential scan was reversed. A scan rate of 1 mV/s was used. These operating conditions were defined for the H_3PO_4 system in order to obtain polarization curves for the determination of the corrosion parameters.

3. Results and discussion

3.1. Materials characterisation

Figure 2 shows the microstructural analysis of the AISI 316L stainless steel tube acquired by scanning electron microscopy (SEM). Microstructural analysis reveals that AISI 316L has a single-phase austenitic microstructure with equiaxed grains. Carbide precipitation was not observed since AISI 316L SS is a stainless steel with low carbon content. AISI 316L SS

microstructure also shows the presence of twins. AISI 316L SS microstructure can also be observed in Figure 3a together with the marks of the diamond pyramid indenter on the alloy surface for microhardness analysis. This photograph was acquired with a light microscope.

Figure 3b shows that the microhardness values of AISI 316L SS are almost constant along the length ring surface and at around 250 HV_{300g}. In general, there is a positive correlation between hardness and strength: the higher the hardness, the higher the strength [35]. Microhardness tests were performed both in etched and untreated samples in order to appreciate any change due to the etching treatment. Microhardness values did not change after etching.

3.2. Influence of impurities on the corrosion of AISI 316L SS

In order to study the influence of impurities (H_2SO_4 and Cl^-) on the corrosion of AISI 316L SS tubes, open circuit potential measurements were carried out in the different solutions. Figure 4 shows the data of the OCP measurements at the different temperatures and Re analysed. According to Figure 4, the open circuit potentials in the pure H_3PO_4 solution tends to shift towards more positive values with time and stabilises during the last minutes of the test. This general tendency of the OCP values can be attributed to surface passivation due to SS high chromium content [14, 16]. As it is well known [36, 37], chromium oxide is considered the main passive component of the passive film in the anodic polarization of stainless steels.

As opposed to OCP in pure H_3PO_4 solutions, open circuit potentials in polluted H_3PO_4 solutions hardly change with time (Figure 4). Moreover, the open circuit potential values of AISI 316L SS in pure phosphoric acid solutions are more positive than the values registered

in the polluted medium. Therefore, impurities seem to reduce passivation, as suggested by Sueptitz et al. [16] who reported that chloride ions hinder the formation of a protective passive film. The corrosive effect of chloride is greatly reinforced by the presence of sulphate ions. Sulphate ions have a synergic effect on corrosion and, for a given chloride content, they greatly increase the speed of corrosion of SS alloys [1, 38]. In spite of this, Figure 4 shows that the evolution of the open circuit potentials in polluted solutions may attain a steady-state after a few minutes of immersion, indicating a good stability of the material/solution system even in the presence of impurities.

Figure 5 shows the cyclic potentiodynamic curves obtained for the materials in pure and polluted H_3PO_4 solutions at the different temperatures and Reynolds numbers analysed. Figure 5 demonstrates that these curves are typical of passivable materials, which proves the good corrosion resistance of austenitic stainless steels in acid media. Typical corrosion parameters such as corrosion current density (i_{corr}) and corrosion potential (E_{corr}) were obtained from these curves. Table 4 shows the mean values of i_{corr} and E_{corr} of AISI 316L SS obtained from the polarization curves. The i_{corr} values obtained in polluted H_3PO_4 solutions are the highest. This fact was also observed by Iken et al. [17]. The presence of aggressive ions in phosphoric acid activated the material surfaces and then accelerated the corrosion rate [17]. In general, the presence of impurities results in more positive corrosion potentials. The shift of E_{corr} towards slightly more positive values could be expected since impurities increase the cathodic reaction rate (see Figure 5). In fact, the cathodic reaction is increased by the larger acid concentration.

Cyclic potentiodynamic curves were carried out to evaluate the repassivation tendency of AISI 316L SS in the different phosphoric acid solutions and operating conditions. Table 5

shows the mean value of the breakdown potentials (E_b) and passivation current densities (i_p) obtained from the anodic branch of the polarization curves. The potential at which the current density reaches 100 $\mu A/cm^2$ was reported as E_b [39]. Passivation current densities were obtained as the mean value between the lowest current density after the transition peak from the active to the passive state and the value where the current density starts to increase drastically with an increase in potential. Table 5 shows that impurities increase passivation current densities and slightly decrease breakdown potential values (less positive). In other words impurities somehow limit the passivation and repassivation characteristics of AISI 316L SS.

Figure 6 represents the difference between E_b and E_{corr} (passivity range). This difference is used as a measure of passivity. The greater the difference, the wider the range of potentials in which the alloys remain passive. The passivity ranges are usually higher for the materials tested in pure phosphoric acid solutions due to the fact that impurities diminish breakdown potentials (less positive values) and shift corrosion potentials to more positive values. These issues also confirm that impurities make passivation of the alloy difficult.

Figure 6 also shows the value of the open circuit potential values (OCP). OCP values were obtained as the arithmetic mean of the last five minute values of open circuit potential measurements [40]. OCP values are in the passive region of the stainless steel in both solutions (pure and polluted), however, in polluted solutions the open circuit potentials are very close to the corrosion potentials, that is, close to the active region.

Figure 7 shows the image of the AISI 316L SS surface after the tests at 60 ºC and at a Re of 5066 acquired by laser scanning confocal microscopy. As it can be observed, the corrosion

process revealed the grain of AISI 316L SS both in pure and polluted H_3PO_4 solutions. The austenitic microstructure of AISI 316L SS could be observed and no considerable differences were found because of the presence of impurities. Figure 7 does not reveal any trace of localized corrosion since no pits can be observed. The photographs show that AISI 316L SS in phosphoric acid solutions undergoes generalized corrosion. This type of corrosion is corroborated by the cyclic potentiodynamic curves of Figure 5, since they did not present a hysteresis loop [41]. This fact shows the clear interest of the alloy for the phosphoric acid industry as a component material of some equipments.

3.3. Influence of temperature on the corrosion of AISI 316L SS

Figure 4 shows that the open circuit potentials tend to shift towards more negative values as temperature increases. More specifically, the most negative OCP values are those corresponding to the highest temperature analysed (see Figure 6). This may indicate that temperature favours the kinetics of corrosion reactions [1, 2]. On the other hand, corrosion current densities increase with temperature (Table 4). This fact also confirms that temperature enhances the corrosion rate [2, 4, 19]. The increase in temperature increases the activity of the aggressive ions adsorbed on the surface, and consequently accelerates the dissolution process and the kinetics of exchange between the electrode surface and the electrolyte [17].

In general, temperature increases the rate of most reactions following Arrhenius equation [42]. In the case of electrochemical reactions, temperature can favour the kinetics of corrosion reactions and, more specifically, the anodic dissolution of the metal [43-45]. The activation energy of the corrosion process can be obtained from Arrhenius-type plots according to the following equation:

$$i_{corr} = A \cdot e^{-\frac{E_a}{R \cdot T}} \quad (3)$$

where E_a is the molar activation energy of the process (J/mol), R is the universal gas constant (8.314 J/(mol K)), T is the temperature (K) and A is a constant. Using the logarithm of the Arrhenius equation the following expression is obtained:

$$Log(i_{corr}) = Log(A) - \frac{E_a}{2.303 \cdot R \cdot T} \quad (4)$$

Therefore, the activation energy values of a corrosion process can be determined from the slope of $log(i_{corr})$ versus 1/T plots [46]. The molar activation energy of an electrochemical process refers to the energy level that must be overcome by one electron in the exchange through the electrode/electrolyte interphase. Moreover, the Arrhenius equation indicates that the greater the dependence of the corrosion rate on temperature, the higher the E_a values [47].

In this electrochemical system, Equation 4 indicates that the higher the slope of the relation between $log(i_{corr})$ and 1/T is, the greater the dependence of the corrosion current density with temperature. Figure 8 shows the plot of the corrosion current density of AISI 316L stainless steel in pure and polluted phosphoric acid solutions versus 1/T, at the different Reynolds numbers studied, according to Equation 4.

Figure 8 shows that the corrosion current density increased with temperature according to Arrhenius equation, in all the solutions analysed. On the other hand, Table 6 includes the relation of $Log(i_{corr})$ and 1/T for the different Re and solutions studied. The higher slope of AISI 316L SS in polluted H_3PO_4 solutions indicates a higher increase of the corrosion current density with temperature in this medium. This means that the most noticeable effect of temperature was in polluted H_3PO_4. Therefore, impurities cause an accelerating corrosion

effect on AISI 316L SS and temperature modifications are more dangerous in polluted acid solutions. The values of the activation energy in both pure and polluted phosphoric acid solutions (around 18 and 35 kJ/mol, respectively) were similar regardless of the Reynolds number studied. This is due to the fact that the i_{corr} values of AISI 316L SS hardly vary with the Reynolds number. Thus, there is no influence of Re on the temperature effects.

As observed in Table 4, corrosion potentials slightly shift towards more positive values in pure phosphoric acid solutions as temperature increases. These results are in good agreement with those reported by other authors [4, 18]. However, corrosion potentials remain almost constant for the stainless steel in polluted phosphoric acid.

With respect to repassivation (Table 5), in general, an increase of temperature induces an increase of the passivation current densities, a decrease of the breakdown potentials (towards more negative values) and a decrease of the passivity range (Figure 6). Consequently, worse passivation and repassivation characteristics could be expected at higher temperatures.

3.4. Influence of Reynolds number on the corrosion of AISI 316L SS

Figures 4 and 6 show that the Reynolds number does not have a great influence on open circuit potential values both in the pure and the polluted phosphoric acid solutions. Similarly, Table 4 shows that corrosion current densities remain almost constant with Re at a certain temperature.

A general dependence of the corrosion rate on fluid velocity could be established in terms of a potential relation between the corrosion rate and the Reynolds number [48-51]:

$$i_{corr} = constant \cdot Re^{a} \quad (5)$$

The experimental exponent "a" in Equation 5 can be in the range 1 to 3 depending upon the corrosion mechanism and flow regime. For simple mass transport to the inside wall of a tube, the value of exponent "a" is close to 1, while for erosion-corrosion in particle-containing liquids, "a" value is up to 3. For values between 1 and 3, there is a mixed control of mass transport and erosion-corrosion. For mixed control of a chemical step and mass transport, "a" value varies between 0 and 1 depending on the mass transport [48, 50-53].

Corrosion current density values of AISI 316L SS have been plotted in Figure 9 according to Equation 5 for all the temperatures analysed in pure and polluted phosphoric acid. Table 7 shows the fitting obtained from the plots of Figure 9. The exponent "a" values seem to be closed to zero in both solutions, independently of temperature.

The value of exponent "a" applied to the Reynolds number, reveals no influence of fluid velocity on the corrosion rate ("a" values = 0). Therefore, it can be concluded that there is a chemical step control of AISI 316L SS corrosion in pure and polluted H_3PO_4 media [48, 50-53].

Similarly, the corrosion potentials (Table 4), the passivation current densities, the breakdown potentials (Table 5) and the passivity ranges (Figure 6) are similar in both solutions regardless of the Reynolds number. Thus no influence of Re on these parameters is expected.

3.5. Combined influence of temperature and Reynolds number on the corrosion of AISI 316L SS

A statistical analysis with Statgraphics software was used to study the combined effects of temperature and Reynolds number on the corrosion behaviour of AISI 316L SS. The effects of temperature (A) and Reynolds number (B) and their respective interactions (AA, BB and AB) on the corrosion parameters (i_{corr}, E_{corr}, i_p and E_b) under hydrodynamic conditions are illustrated in the Pareto charts and response surface graphs in Figures 10 and 11, for pure and polluted phosphoric acid, respectively.

Pareto charts represent the influence of each factor (temperature, Re or their interactions) as a function of the standardized effect, which is proportional to the magnitude of the effect on the corrosion parameter studied in each case. Figures 10 (pure) and 11 (polluted) show that the effect of temperature (A) is significant on all corrosion parameters except on the corrosion potential, with a P-value of less than 0.05. Temperature increases i_{corr} and i_p (positive effect) and decreases E_b (negative effect). The effect of temperature seems to be of the same magnitude order for the corrosion potential, the passivation current density and the breakdown potential, independently of the presence of impurities, since the standardized effects are similar. However, the effect of temperature on the corrosion current density is much more important than on the rest of the corrosion parameters analysed, especially in polluted phosphoric acid solutions. This effect might be due to the presence of impurities, as corroborated by the results of the Arrhenius plot, where a higher slope of the relation Log(i_{corr}) vs 1/T was obtained in polluted phosphoric acid media. On the other hand, the effect of Reynolds number (B) on the corrosion parameters is not significant, since it does not reach the vertical line that defines 95% of the confidence interval.

The response surface graphs shown in Figures 10 and 11 confirm the behaviour observed in the Pareto charts. In all of them, the inclined surfaces that generate the most significant

variation in the corrosion parameters are induced by an increase in temperature, rather than by the Reynolds number. Furthermore, the surface generated by the corrosion potential is practically horizontal; this corroborates that both the effect of temperature and Reynolds number was not significant on this parameter.

4. Conclusions

This work studies the influence of temperature (25 to 60 ºC) and hydrodynamic conditions (Reynolds numbers from 1456 to 5066) on the corrosion of AISI 316L stainless steel in pure and polluted phosphoric acid solutions using cyclic polarization curves. A hydrodynamic circuit was employed to perform the tests. Furthermore, statistical analysis by the response surface methodology has proved to be a useful tool to analyse the combined effects of operating conditions on the corrosion parameters. The main conclusions drawn from the research are summarized as follows:

1. Impurities increase the corrosion rate and hinder the passivation and repassivation resistance of AISI 316L SS since they increase i_{corr} and i_p, and diminish passivity ranges, shifting E_b towards more negative values.

2. Temperature increases the corrosion rate and consequently worsens passivation and repassivation properties of the alloy.

3. Arrhenius plot shows that impurities increase the value of the activation energy. Therefore, impurities cause an accelerating corrosion effect on AISI 316L SS and temperature modifications will be more dangerous in polluted acid solutions. The

value of the activation energy in both pure and polluted phosphoric acid solutions was very similar regardless of the Reynolds number studied.

4. Reynolds number seems to have no influence on the corrosion rate and repassivation parameters.

5. There is a chemical step control of AISI 316L stainless steel corrosion in pure and polluted H_3PO_4 media, since exponent “a” applied to the Reynolds number is close to zero.

6. Response surface methodology analysis shows that in the range of temperatures and Reynolds numbers studied the effect of temperature on the corrosion parameters is much higher than that of the Reynolds number. Moreover, the effect of temperature on the corrosion rate is enhanced by the presence of impurities in the acid medium.

7. AISI 316L stainless steel has proved to be an excellent component material of some equipment in the phosphoric acid industry due to its good corrosion properties at the different temperatures and Reynolds numbers studied, even in polluted media. The corrosion rate should be specially controlled when temperature is modified in the presence of impurities, in this way, economic losses due to corrosion could be reduced and environmental resources could be saved.

Acknowledgements: the authors would like to express their gratitude to the Spanish MAEC (PCI Mediterráneo C/8196/07, C/018046/08, D/023608/09, D/030177/10), to the Generalitat Valenciana for its help in the CLSM acquisition (MY08/ISIRM/S/100) and to Dr. Asunción Jaime for her translation assistance.

TABLE CAPTIONS

Table 1. Composition of the different phosphoric acid solutions used.

Table 2. Density and viscosity values of the phosphoric acid solutions.

Table 3. Flow rates used for the different H_3PO_4 solutions.

Table 4. Corrosion current densities (i_{corr}) and corrosion potentials (E_{corr}) of AISI 316L SS at the different temperatures and Reynolds numbers analysed for pure and polluted H_3PO_4 solutions.

Table 5. Passivation current densities (i_p) and breakdown potentials (E_b) of AISI 316L SS at the different temperatures and Reynolds numbers analysed for pure and polluted H_3PO_4 solutions.

Table 6. Fitting of the Arrhenius plot and activation energy values at the different Reynolds numbers analysed for pure and polluted H_3PO_4 solutions.

Table 7. Fitting of the corrosion current density vs Reynolds number plots at the different Reynolds numbers analysed for pure and polluted H_3PO_4 solutions.

FIGURE CAPTIONS

Figure 1. Schematic diagram of the hydrodynamic circuit used to perform the tests.

Figure 2. Microstructure of AISI 316L SS acquired by SEM.

Figure 3. Microstructure of AISI 316L SS acquired by LM with the marks of the diamond pyramid indenter (a) and microhardness values of the alloy (b).

Figure 4. Open circuit potential register of AISI 316L SS in pure H_3PO_4 solutions (solid line) and in polluted H_3PO_4 solutions (broken line) at the different temperatures and Reynolds numbers studied.

Figure 5. Cyclic potentiodynamic curves of AISI 316L SS in pure and polluted phosphoric acid at different temperatures and Reynolds numbers.

Figure 6. Passivity ranges of AISI 316L SS in the different H_3PO_4 solutions at the temperatures and Reynolds numbers studied. Cross points indicate the OCP values.

Figure 7. Photographs of AISI 316L SS surface after the tests at Reynolds number of 5066 and at 60 ºC in pure H_3PO_4 (a) and polluted H_3PO_4 (b), acquired by LSCM.

Figure 8. Dependence of the corrosion current of AISI 316L SS on the temperature according to Arrhenius plot at the different Reynolds numbers studied, for pure and polluted phosphoric acid solutions. P = pure H_3PO_4 and Pol = polluted H_3PO_4 (Reynolds number).

Figure 9. Variation of AISI 316L SS corrosion current density with Reynolds number at all the temperatures studied, for pure and polluted phosphoric acid solutions. P = pure H_3PO_4 and Pol = polluted H_3PO_4 (Reynolds number).

Figure 10. Pareto charts and response surface graphs of the different corrosion parameters for pure H_3PO_4 solutions. a) influence on i_{corr}; b) influence on E_{corr}; c) influence on i_p; d) influence on E_b. In Pareto charts the vertical line defines 95% of the confidence intervals.

Figure 11. Pareto charts and response surface graphs of the different corrosion parameters for polluted H_3PO_4 solutions. a) influence on i_{corr}; b) influence on E_{corr}; c) influence on i_p; d) influence on $E_{b.}$ In Pareto charts the vertical line defines 95% of the confidence intervals.

References

[1] P. Becker, Phosphates and phosphoric acid. Raw materials, technology, and economics of the wet process, second ed., Marcel Dekker, New York, 1989.

[2] A. Guenbour, H. Iken, N. Kebkab, A. Bellaouchou, R. Boulif, A. Benbachir, Appl. Surf. Sci. 252 (2006) 8710-8715.

[3] T.Y. Chen, A.A. Moccari, D.D. Macdonald, Corrosion 48 (1992) 239-255.

[4] A. Guenbour, M.A. Hajji, El M. Jallouli, A. BenBachir, Appl. Surf. Sci. 253 (2006) 2362-2366.

[5] M. Schorr, B. Valdez, R. Slatev, M. Stoytcheva, Mater. Perform. 49 (2010) 56-59.

[6] Corrosion costs and preventive strategies in United States of America. NACE Internacional (National Association of Corrosion Engineers). http://events.nace.org/publicaffairs/images_cocorr/ccsupp.pdf, (2007).

[7] M.F. De Riccardis, V. Martina, D. Carbone, M. Re, E. Pesce, R. Terzi, B. Bozzini, Mater. Chem. Phys. 125 (2011) 271-276.

[8] L. Narváez, E. Cano, D.M. Bastidas, J. Appl. Electrochem. 35 (2005) 499-506.

[9] A.S. Hamdy, B. Marx, D. Butt, Mater. Chem. Phys. 126 (2011) 507-514.

[10] B. Arifvianto, Suyitno, M. Mahardika, P. Dewo, P.T. Iswanto, U.A. Salim, Mater. Chem. Phys. 125 (2011) 418-426.

[11] H. Buscail, S. El Messki, F. Riffard, S. Perrier, R. Cueff, E. Caudron, C. Issartel, Mater. Chem. Phys. 111 (2008) 491-496.

[12] A.I. Almarshad, D. Jamal, J. Appl. Electrochem.34 (2004) 67-70.

[13] J. Oñoro, Int. J. Pres. Ves. Pip. 86 (2009) 656-660.

[14] S. El Hajjaji, L. Aries, J. Audouard, F. Dabosi, Corros. Sci. 37 (1995) 927-939.

[15] A. Guenbour, M. Essahli, A. Benbachir, L. Aries, R. Boulif, Acta Chim. Slov. 50 (2003) 287-299.

[16] R. Sueptitz, M. Uhlemann, A. Gebert, L. Schultz, Corros. Sci. 52 (2010) 886-891.

[17] H. Iken, R. Basseguy, A. Guenbour, A. BenBachir, Electrochim. Acta 52 (2007) 2580-2587.

[18] A. Bellaouchou, A. Guenbour, A. BenBachir, Corrosion 49 (1993) 656-662.

[19] M. Benabdellah, B. Hammouti, Appl. Surf. Sci. 252 (2005) 1657-1661.

[20] M. Khadiri, A. Benyaïch, A. Outzourhit, E.L. Ameziane, Ann. Chim.-Sci. Mat. 25 (2000) 447-455.

[21] P.R. Roberge, Corrosion Engineering Principles and Practice, first ed., McGrawHill USA, 2008.

[22] N. Pérez, Electrochemistry and Corrosion Science, first ed., Kluwer USA, 2004.

[23] Y.L. Pang, A.Z. Abdullah, S. Bhatia, Chem. Eng. J. 166 (2011) 873-880.

[24] K.H. Goh, T.T. Lim, P.C. Chui, Corros. Sci. 50 (2008) 918-927.

[25] S. Rajakumar, C. Muralidharan, V. Balasubramanian, Mater. Des. 32 (2011) 2878-2890.

[26] M. Masmoudi, D. Capek, R. Abdelhedi, F. El Halouani, M. Wery, Surf. Coat. Tech. 200 (2006) 6651-6658.

[27] G.F. Vander Voort, Metallography. Principles and practice, second ed., ASM International, USA, 1999.

[28] ASTM E-384, Standard test method for microindentation hardness of materials, ASTM International, Pennsylvania, 1999.

[29] E.P. Egan, B.B. Luff, J. Ind. Eng. Chem. 47 (1955) 1280-1281.

[30] R.C. Weast, D.R. Lide, M.J. Astle, W.H. Beyer, CRC Handbook of chemistry and physics, seventieth ed., CRC Press Inc USA, 1990.

[31] R.H. Perry y D.W. Green, Perry's Chemical Engineers' handbook, seventh ed., McGraw-Hill USA, 1999.

[32] M. Laliberté, W.E. Cooper, J. Chem. Eng. Data 49 (2004) 1141-1151.

[33] ASTM D445-09 Standard Test Method for Kinematic Viscosity of Transparent and Opaque Liquids (and Calculation of Dynamic Viscosity), Pennsylvania, 2009.

[34] ASTM D446-07 Standard Specifications and Operating Instructions for Glass Capillary Kinematic Viscometers, Pennsylvania, 2007.

[35] T.-Y. Kuo, H.-T. Lee, Mater. Sci. Eng. A 338 (2002) 202-212.

[36] M. Abdallah, Mater. Chem. Phys. 82 (2003) 786-792.

[37] S.K. Yen, Y.C. Tsai, J. Electrochem. Soc. 143 (1996) 2493-2497.

[38] T. Theys, Influence of the rock impurities on the phosphoric acid process, products and some downstream uses, IFA meeting, Abu Dhabi, 2003.

[39] M. Kaneko, H.S. Isaacs, Corros. Sci. 42 (2000) 67-78.

[40] ASTM G-5, Test method for making potenciostatic and potenciodynamic anodic polarization measurements, Pennsylvania, 2004.

[41] A. Pardo Gutierrez del Cid, E. Otero Huerta, M.C. Merino Casals, M.D. Lopez Gonzalez, M.W. Utrilla Esteban, Rev. Metal. Madrid 27 (2001) 499-508.

[42] A.J. Bard, L.R. Faulkner, Electrochemical methods. Fundamentals and Applications, second ed., John Wiley & Sons, Inc, USA, 2001.

[43] L.F. Garfias-Mesias, J.M. Sykes, Corros. Sci. 41 (1999) 959-987.

[44] N.J. Laycock, Corrosion 55 (1999) 590-595.

[45] A. Pardo, E. Otero, M.C. Merino, M.D. López, M. V. Utrilla, F. Moreno, Corrosion 56 (2000) 411-418.

[46] R.M. El Sherif, K.M. Ismail, W.A. Badawy, Electrochim. Acta 49 (2004) 5139-5150.

[47] P.W. Atkins, Physical Chemistry, sixth ed., Oxford University Press, USA, 1998.

[48] E. Heitz, Electrochim. Acta 41 (1996) 503-509.

[49] E. Heitz, Corrosion 47 (1991) 135-145.

[50] M.M. Stack, F.H. Stott, G.C. Wood, J. Phys. IV 3 (1993) 687-694.

[51] J.R. Shadley, S.A. Shirazi, E. Dayalan, E.F. Rybicki, Corrosion 54 (1998) 972-978.

[52] M.M. Stack, J.G. ChaconNava, F.H. Stott, Mater. Sci. Tech. 11 (1995) 1180-1185.

[53] J.R. Shadley, S.A. Shirazi, E. Dayalan, M. Ismail, E.F. Rybicki, Corrosion 52 (1996) 714-723.

Table 1

	H_3PO_4	H_2SO_4	Cl^-
Pure acid	40 wt. % (5.5 M)	-	-
Polluted acid	40 wt. % (5.5 M)	2 wt. %	380 ppm

Table 2

	T (°C)	Pure H_3PO_4	Polluted H_3PO_4	
Density (g/mL)	25	**1.2527**[29]	**1.2615**	ρ_H_2O = 0.99707[30]
				ρ_H_3PO_4 (84 wt. %) = 1.6733[29]
				ρ_H_2SO_4 (98 wt. %) = 1.8310[31]
				ρ_KCl (2 wt. %) = 1.00977[31]
	40	**1.2444**[29]	**1.2543**	ρ_H_2O = 0.99224[30]
				ρ_ H_3PO_4 (84 wt. %) = 1.6615[29]
				ρ_H_2SO_4 (98 wt. %) = 1.8163[31]
				ρ_KCl (2 wt. %) = 1.00471[31]
	60	**1.2326**[29]	**1.2426**	ρ_H_2O = 0.98324[30]
				ρ_ H_3PO_4 (84 wt. %) = 1.6456[29]
				ρ_H_2SO_4 (98 wt. %) = 1.7976[31]
				ρ_KCl (2 wt. %) = 0.99560[31]
Viscosity (cP)	25	**3.7244**	**3.7335**	
	40	**2.6140**	**2.6298**	
	60	**1.7666**	**1.7742**	

Table 3

	Flow rates (L/h)					
	Pure H_3PO_4			Polluted H_3PO_4		
T (ºC)	**Re = 1456**	**Re = 3166**	**Re = 5066**	**Re = 1456**	**Re = 3166**	**Re = 5066**
25	171	373	596	171	371	594
40	121	263	421	121	263	420
60	83	180	287	82	179	286

Table 4

Re	Temperature	i_{corr} ($\mu A/cm^2$)		E_{corr} ($mV_{Ag/AgCl}$)	
		Pure H_3PO_4	**Polluted H_3PO_4**	**Pure H_3PO_4**	**Polluted H_3PO_4**
1456	25 ºC	4.92 ± 0.10	7.45 ± 0.42	-282 ± 1	-224 ± 14
	40 ºC	6.41 ± 0.12	18.03 ± 1.04	-251 ± 7	-213 ± 21
	60 ºC	10.18 ± 0.19	32.68 ± 0.59	-250 ± 4	-220 ± 6
3166	25 ºC	4.43 ± 0.32	7.33 ± 0.37	-275 ± 15	-241 ± 21
	40 ºC	6.50 ± 0.31	18.27 ± 1.03	-262 ± 21	-223 ± 20
	60 ºC	10.23 ± 0.79	32.85 ± 0.41	-254 ± 15	-221 ± 13
5066	25 ºC	4.60 ± 0.22	7.59 ± 0.76	-268 ± 6	-211 ± 5
	40 ºC	6.53 ± 0.33	18.53 ± 0.61	-270 ± 20	-211 ± 1
	60 ºC	10.19 ± 0.44	32.77 ± 1.65	-209 ± 19	-218 ± 11

Table 5

Re	Temperature	i_p ($\mu A/cm^2$)		E_b ($mV_{Ag/AgCl}$)	
		Pure H_3PO_4	**Polluted H_3PO_4**	**Pure H_3PO_4**	**Polluted H_3PO_4**
1456	25 ºC	5.68 ± 0.45	8.00 ± 0.49	1158 ± 14	1140 ± 1
	40 ºC	8.67 ± 1.02	11.55 ± 0.28	1124 ± 1	1099 ± 3
	60 ºC	7.25 ± 1.45	14.52 ± 0.98	1083 ± 9	1076 ± 14
3166	25 ºC	6.04 ± 1.00	9.11 ± 1.05	1162 ± 4	1136 ± 8
	40 ºC	8.18 ± 1.20	11.28 ± 0.54	1115 ± 14	1110 ± 4
	60 ºC	7.23 ± 1.03	13.17 ± 0.83	1094 ± 6	1075 ± 6
5066	25 ºC	5.45 ± 1.00	7.31 ± 1.01	1159 ± 1	1133 ± 3
	40 ºC	8.36 ± 1.06	10.54 ± 1.11	1105 ± 4	1115 ± 3
	60 ºC	7.42 ± 0.89	12.59 ± 1.05	1096 ± 11	1093 ± 10

Table 6

Re	Pure H_3PO_4	Polluted H_3PO_4
1456	$Log(i_{corr}) = 3.70 - 900.16 \cdot (1/T)$ $E_a = 17.24$ kJ/mol	$Log(i_{corr}) = 6.96 - 1805.00 \cdot (1/T)$ $E_a = 34.56$ kJ/mol
3166	$Log(i_{corr}) = 4.10 – 1029.10 \cdot (1/T)$ $E_a = 19.70$ kJ/mol	$Log(i_{corr}) = 7.04 - 1830.70 \cdot (1/T)$ $E_a = 35.05$ kJ/mol
5066	$Log(i_{corr}) = 3.96 - 981.83 \cdot (1/T)$ $E_a = 18.80$ kJ/mol	$Log(i_{corr}) = 6.90 - 1784.30 \cdot (1/T)$ $E_a = 34.16$ kJ/mol

Table 7

T (ºC)	Pure H_3PO_4	Polluted H_3PO_4
25	$i_{corr} = 7.65 \cdot Re^{-0.0626}$	$i_{corr} = 6.82 \cdot Re^{0.0113}$
40	$i_{corr} = 5.76 \cdot Re^{0.0149}$	$i_{corr} = 15.44 \cdot Re^{0.0212}$
60	$i_{corr} = 10.07 \cdot Re^{0.0016}$	$i_{corr} = 32.08 \cdot Re^{0.0027}$

Figure 1

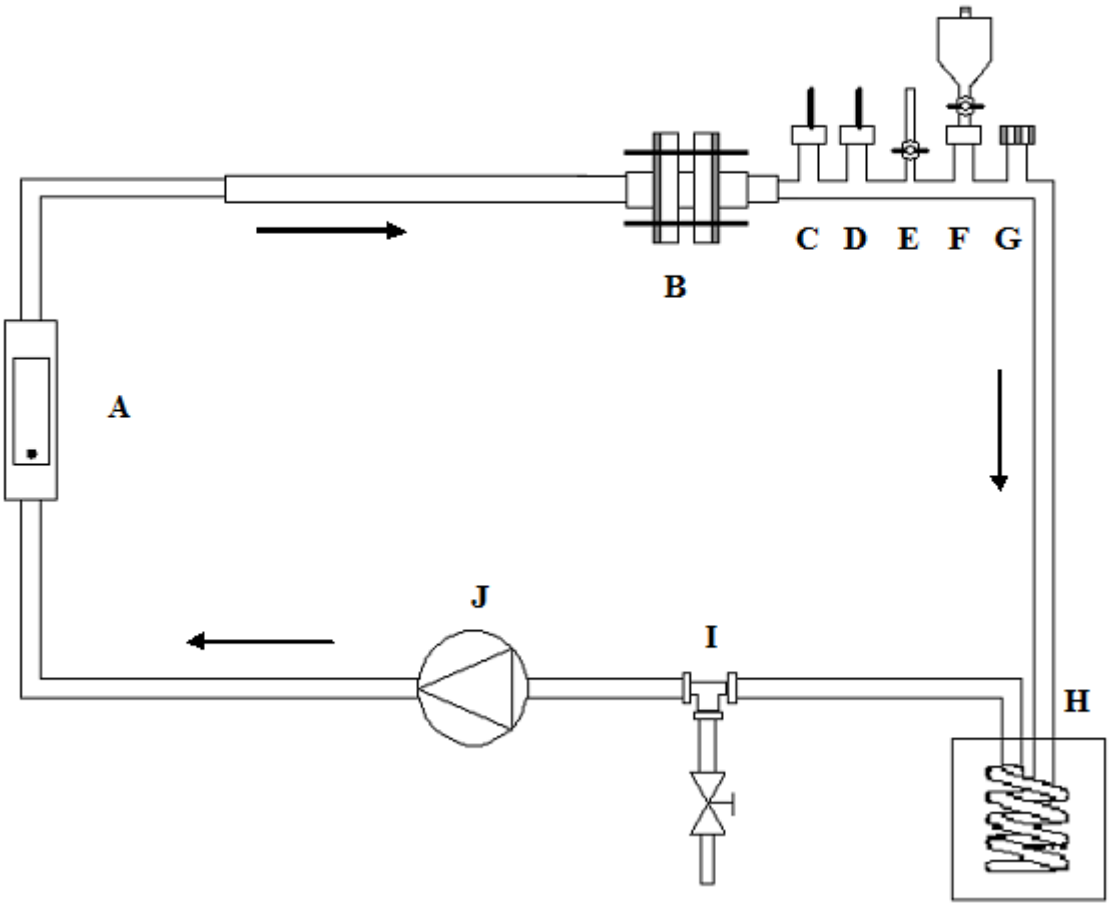

Figure 2

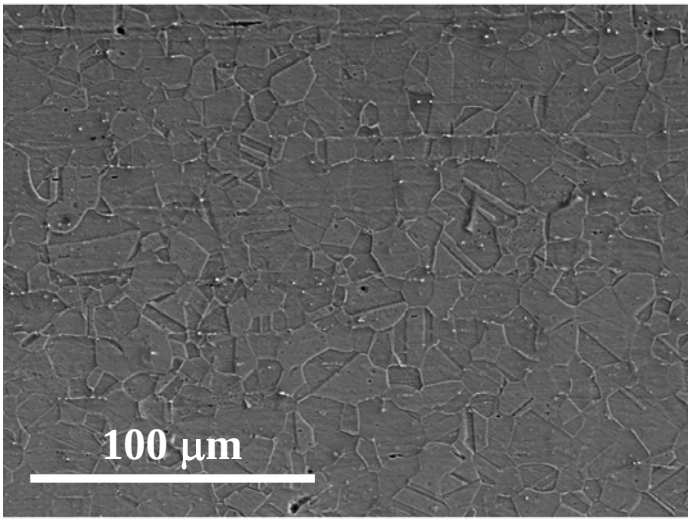

Figure 3

a

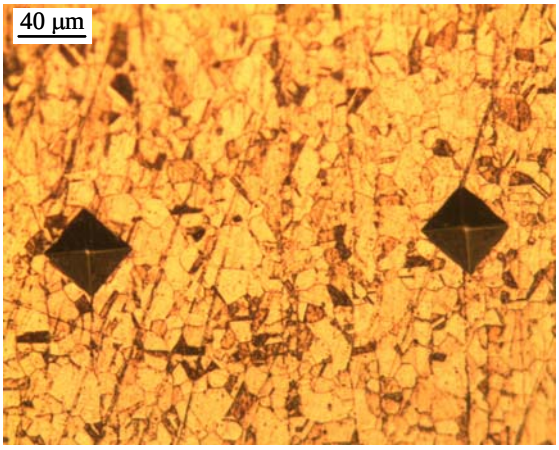
40 µm

b

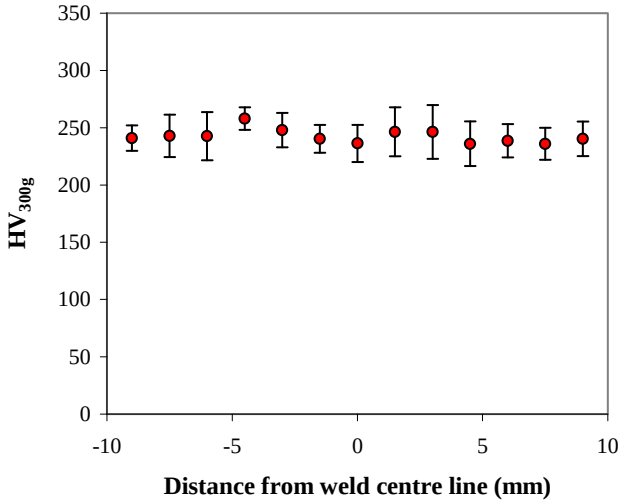
350
300
250
200
150
100
50
0
HV300g
-10
-5
0
5
10
Distance from weld centre line (mm)

Figure 4

Re = 1456

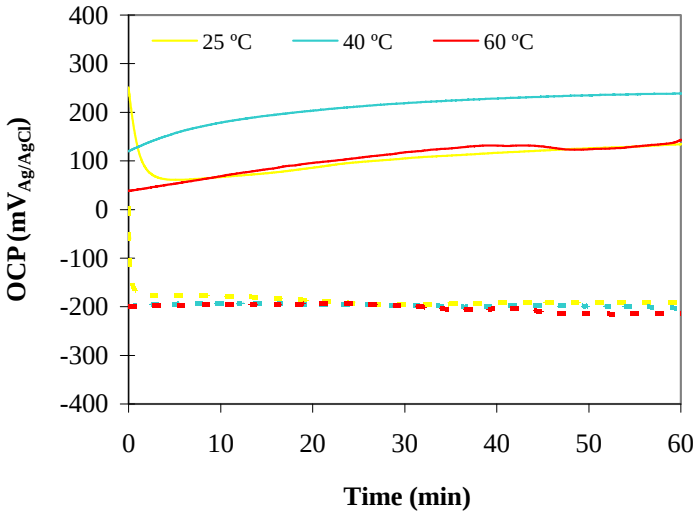

Re = 3166

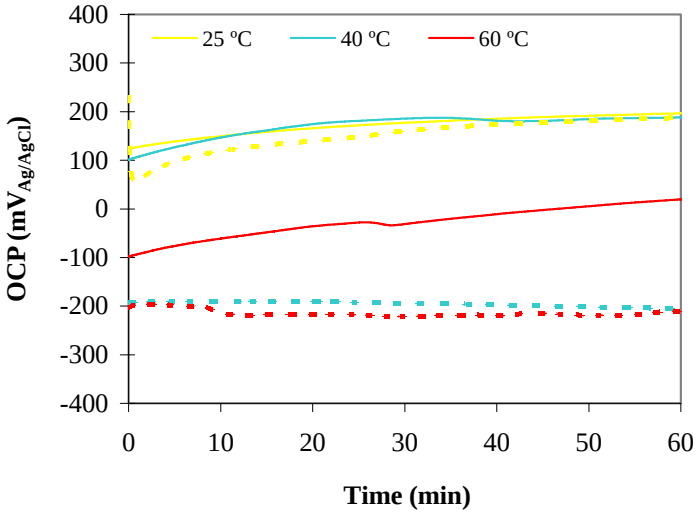

Re = 5066

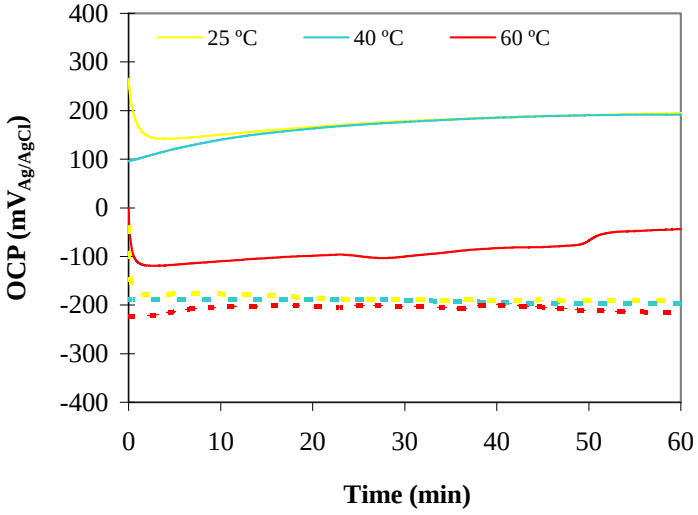

Figure 5

T / Re	25 ºC	40 ºC	60 ºC
1456	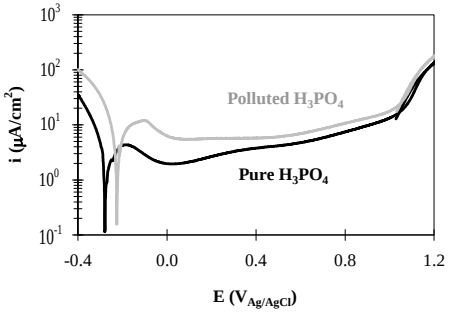	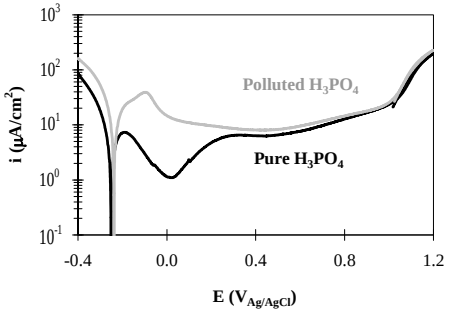	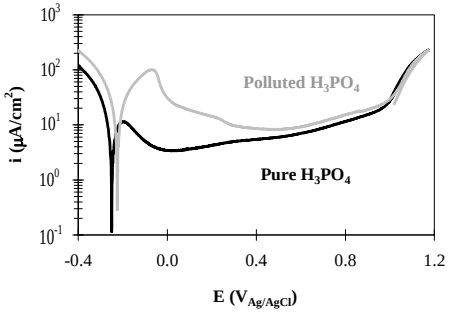
3166	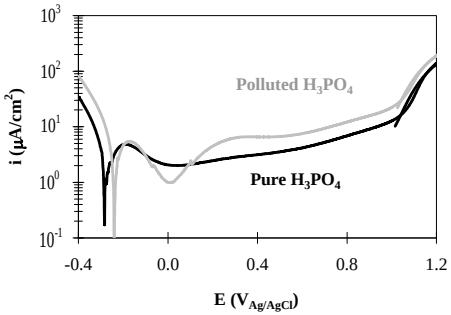	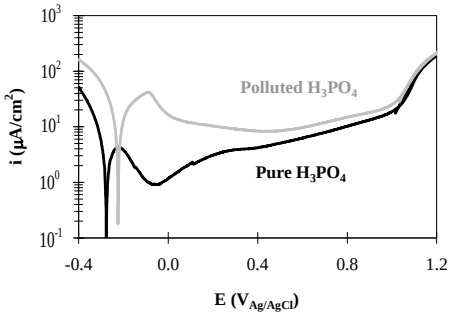	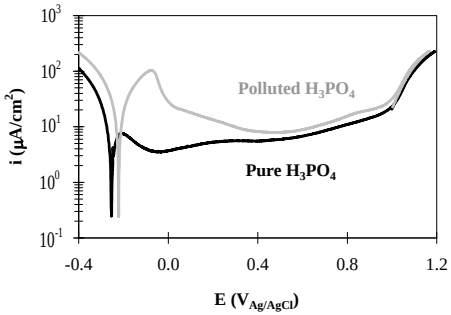
5066	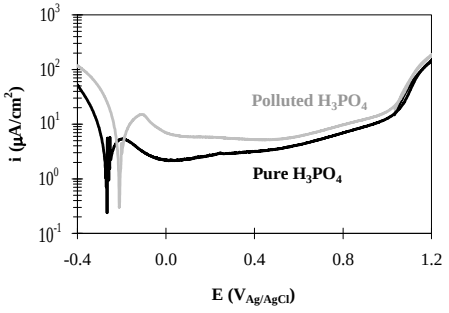	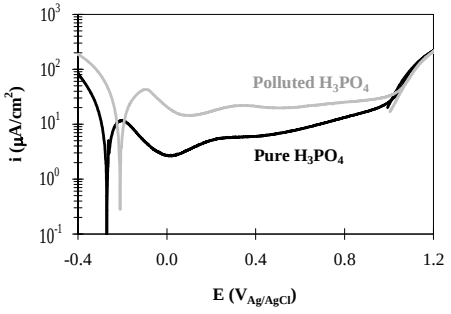	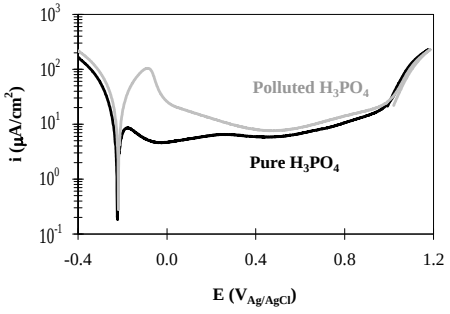

Figure 6

Re = 1456

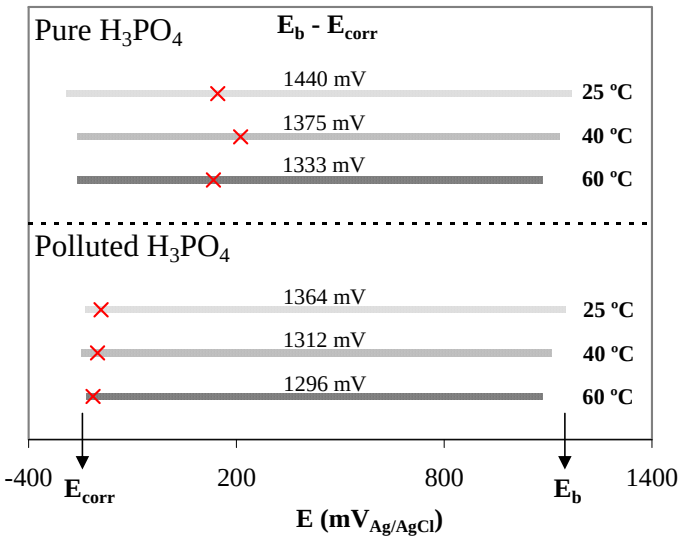

Re = 3166

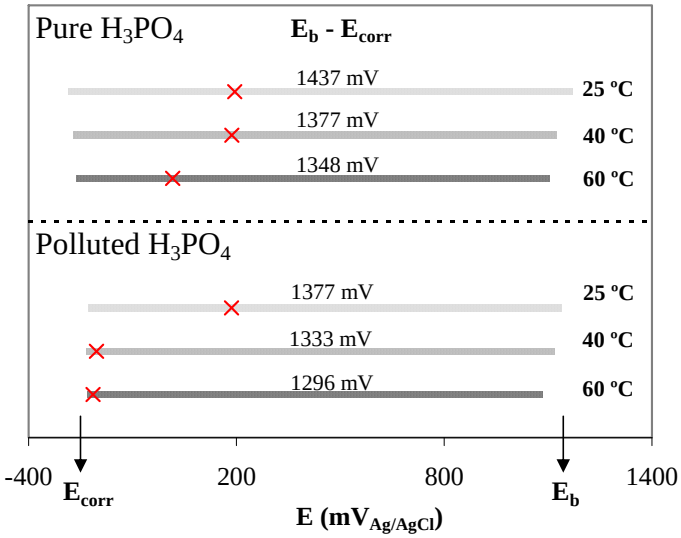

Re = 5066

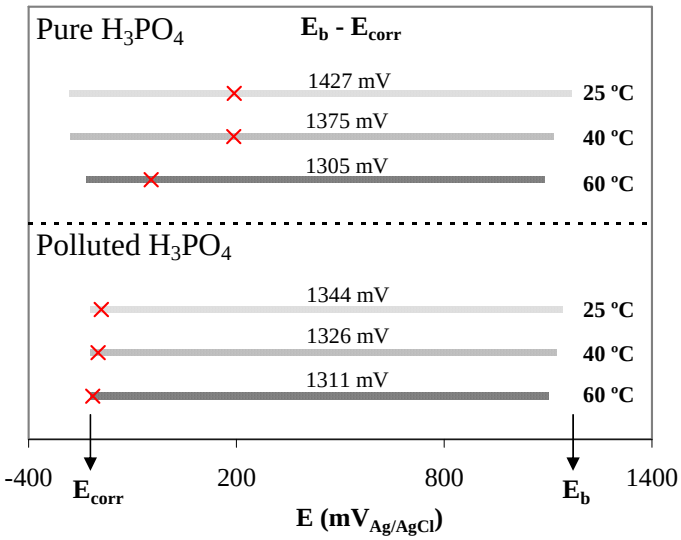

Figure 7

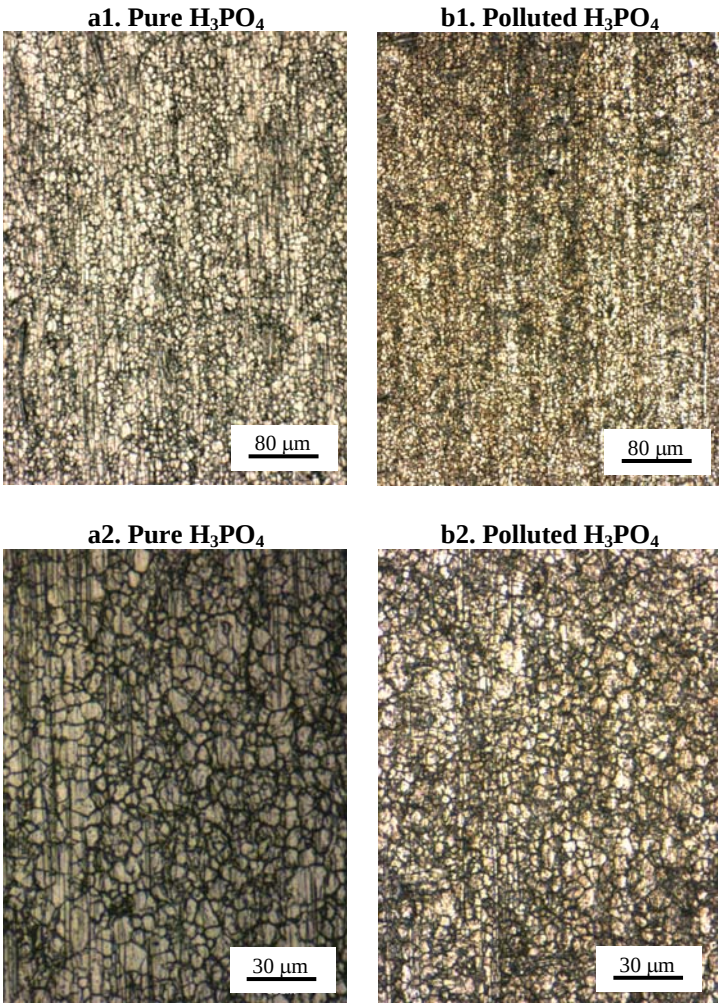
a1. Pure H_3PO_4
b1. Polluted H_3PO_4
80 μm
80 μm
a2. Pure H_3PO_4
b2. Polluted H_3PO_4
30 μm
30 μm

Figure 8

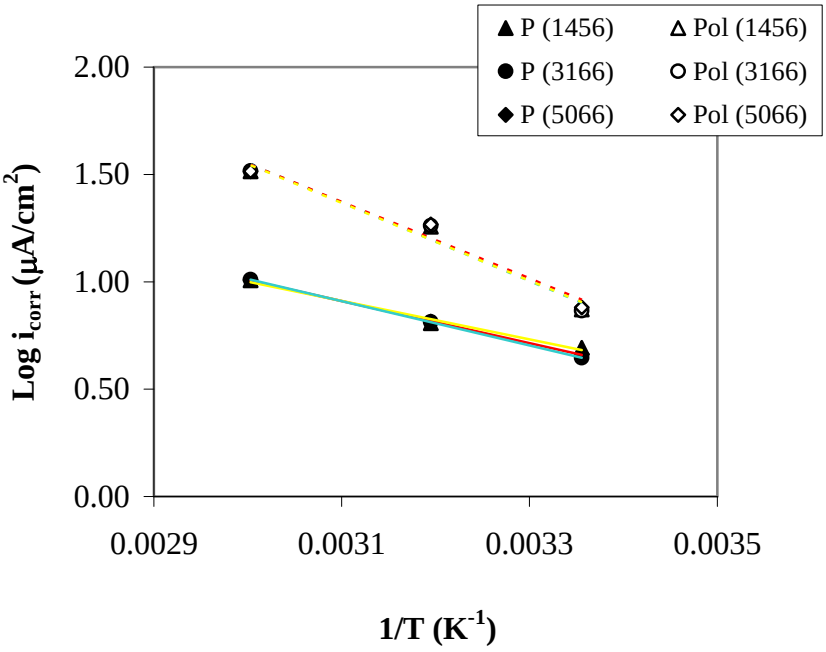
P (1456)
Pol (1456)
P (3166)
Pol (3166)
P (5066)
Pol (5066)
2.00
1.50
1.00
0.50
0.00
0.0029
0.0031
0.0033
0.0035
Log i_corr (µA/cm²)
1/T (K⁻¹)

Figure 9

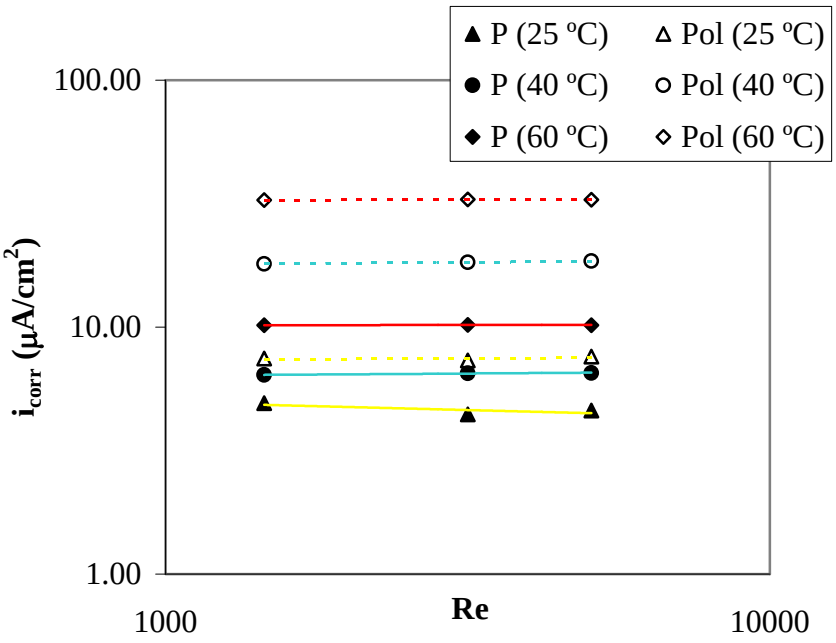
P (25 ºC)
Pol (25 ºC)
P (40 ºC)
Pol (40 ºC)
P (60 ºC)
Pol (60 ºC)
100.00
10.00
1.00
i_{corr} (µA/cm^2)
1000
Re
10000

Figure 10

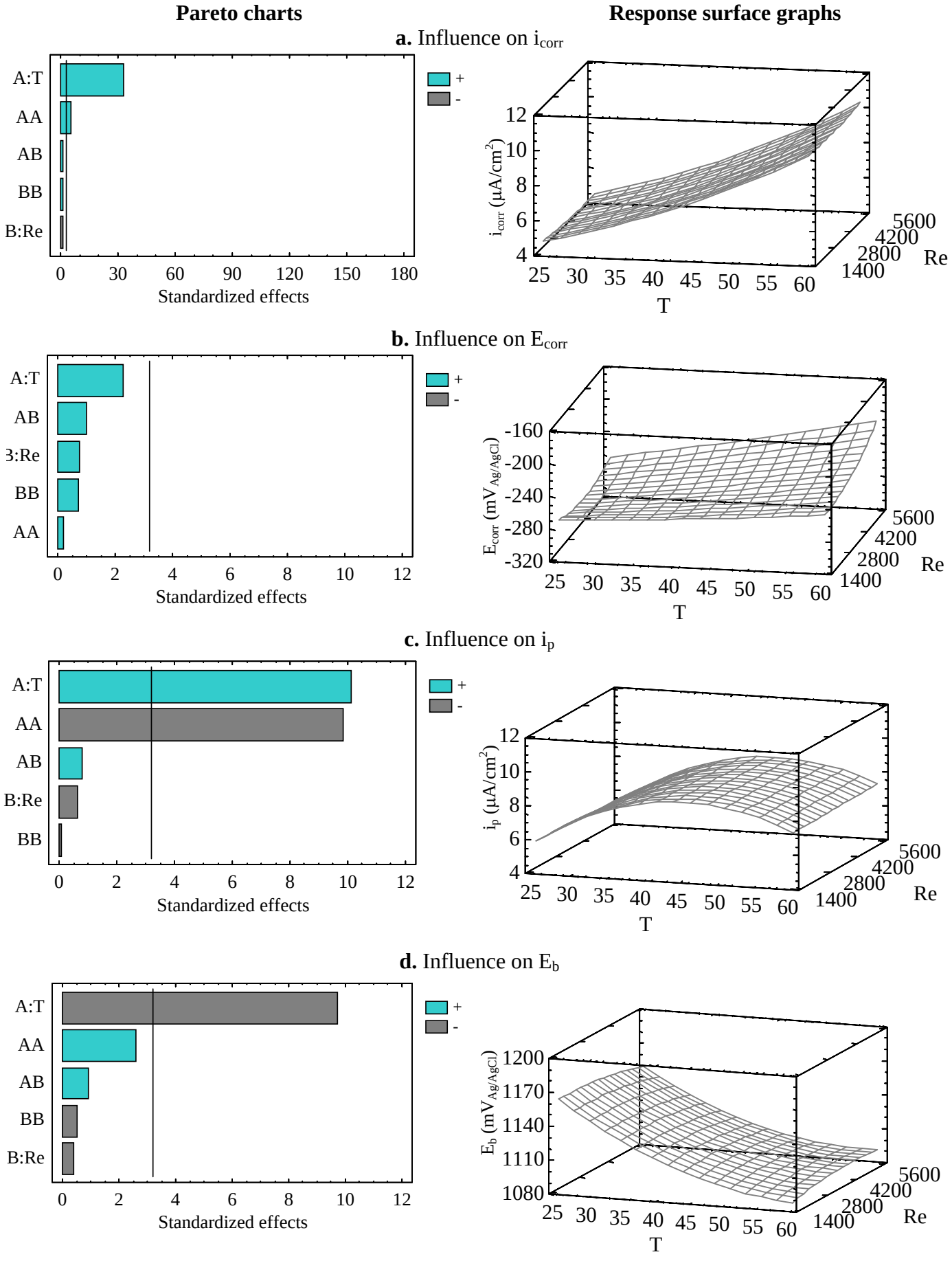
Pareto charts
Response surface graphs
a. Influence on i_{corr}
A:T
AA
AB
BB
B:Re
+
-
0 30 60 90 120 150 180
Standardized effects
i_{corr} ($\mu A/cm^2$)
12 10 8 6 4
25 30 35 40 45 50 55 60
T
5600 4200 2800 1400
Re
b. Influence on E_{corr}
A:T
AB
3:Re
BB
AA
0 2 4 6 8 10 12
Standardized effects
E_{corr} ($mV_{Ag/AgCl}$)
-160 -200 -240 -280 -320
25 30 35 40 45 50 55 60
T
5600 4200 2800 1400
Re
c. Influence on i_p
A:T
AA
AB
B:Re
BB
0 2 4 6 8 10 12
Standardized effects
i_p ($\mu A/cm^2$)
12 10 8 6 4
25 30 35 40 45 50 55 60
T
5600 4200 2800 1400
Re
d. Influence on E_b
A:T
AA
AB
BB
B:Re
0 2 4 6 8 10 12
Standardized effects
E_b ($mV_{Ag/AgCl}$)
1200 1170 1140 1110 1080
25 30 35 40 45 50 55 60
T
5600 4200 2800 1400
Re

Figure 11

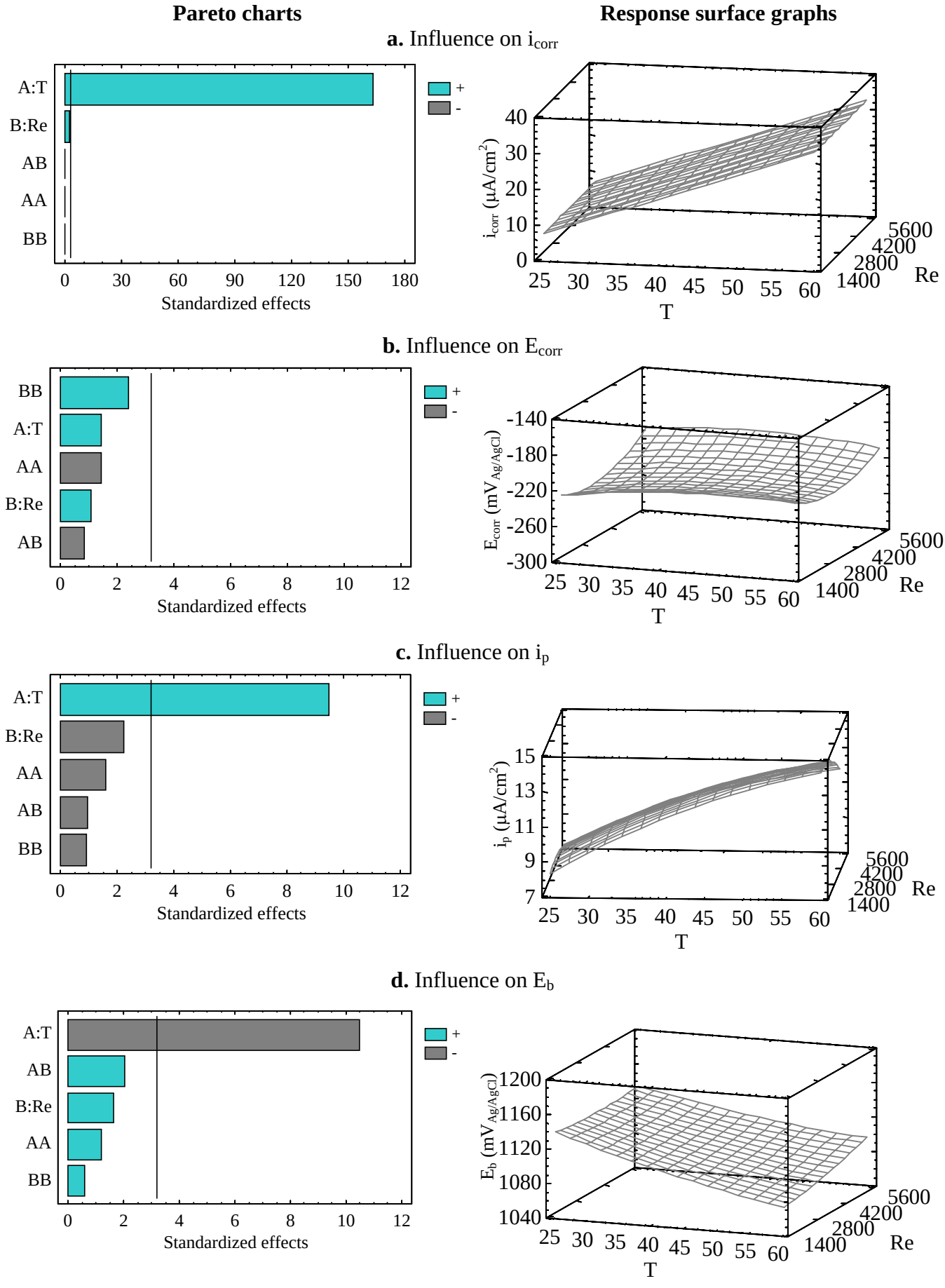
Pareto charts
Response surface graphs
a. Influence on i_{corr}
A:T
B:Re
AB
AA
BB
+
-
0 30 60 90 120 150 180
Standardized effects
i_{corr} (µA/cm^2)
0 10 20 30 40
25 30 35 40 45 50 55 60
T
1400 2800 4200 5600
Re
b. Influence on E_{corr}
BB
A:T
AA
B:Re
AB
0 2 4 6 8 10 12
Standardized effects
E_{corr} (mV$_{Ag/AgCl}$)
-140 -180 -220 -260 -300
c. Influence on i_p
i_p (µA/cm^2)
7 9 11 13 15
d. Influence on E_b
E_b (mV$_{Ag/AgCl}$)
1040 1080 1120 1160 1200